Astron. Astrophys. 343, 720–732 (1999)

ASTRONOMY
AND
ASTROPHYSICS

The metallicity distribution and the G-dwarf problem in elliptical galaxies

L. Angeletti and P. Giannone

Istituto Astronomico, Università 'La Sapienza', Via Lancisi 29, I-00161 Roma, Italy

Received 12 May 1998 / Accepted 22 November 1998

Abstract. We investigate distributions of the stellar metallicity Z which can solve the local (within the effective radius) and/or the global G-dwarf problem in elliptical galaxies. We represent an elliptical galaxy with the spherical and isotropic model by Hernquist (1990) and relate the Z dispersion to the stellar binding energy $\mathcal{E}$. Such a $Z-\mathcal{E}$ relation may be a single-valued function $Z(\mathcal{E})$, or an $\mathcal{E}$-dependent Z spectrum for each value of $\mathcal{E}$ in its proper range. In this preliminary paper we only consider a stellar component of one age, thus disregarding a superposition of several independent $Z-\mathcal{E}$ relations. Moreover, we adopt an exploratory approach with the aid of a few simple $Z-\mathcal{E}$ relations, and take into account the observed colours and metallicity radial gradients together with the $(U-V)-(V-K)$ and $(1550-V)-Mg_2$ correlations. We find that some of the adopted $Z-\mathcal{E}$ relations fit reasonably well the observed correlations and, at the same time, can solve the local and/or the global G-dwarf problem. In particular, the 'Simple Model' can remove the local G-dwarf problem but not the global one, whereas the 'Best Accretion Model' by Lynden-Bell (1975) can avoid both problems. Furthermore, our results suggest a viable approach to the formulation of a flexible $Z-\mathcal{E}$ relation, either as a single-valued $Z(\mathcal{E})$ or an $\mathcal{E}$-dependent Z spectrum, that can solve the G-dwarf problem and agree with all the major observational evidences. We confirm that the mean metallicities, as inferred from the Single Stellar Populations and observed colours or spectral indices (e.g. Mg_2), may be underestimated by up to a factor of two, owing to the stellar metallicity spread in real ellipticals.

Key words: ultraviolet: galaxies – galaxies: stellar content – galaxies: elliptical and lenticular, cD – galaxies: abundances

1. Introduction

In the last few years some authors have shown that the number of metal-poor stars in elliptical galaxies is less than predicted by the so-called Simple Model (SM) of chemical evolution (for the SM see e.g. Pagel & Patchett 1975, Pagel 1989, 1997). Firstly, Bressan et al. (1994) and Tantalo et al. (1996, hereafter TCBF) found that the closed-box approximation predicts an excess of light, in the 2000 to 3500 Å spectral region, with respect to the observed integrated spectral energy distribution in ellipticals (e.g. M32 and NGC 4649). Such an excess can only be cured by suppressing the contribution from stars with a metal abundance (by mass) $Z < 0.008$, i.e. $Z < 0.5Z_{\odot}$ with our adopted $Z_{\odot} = 0.0169$. An analogous flux excess is also found for the bulge of M31 (Worthey et al. 1996). Secondly, star counts in a region $1' - 2'$ from the center of M32 and based on HST observations (Grillmair et al. 1996) showed that the stellar Z distribution is similar to, and perhaps narrower than, the one found in the solar neighbourhood (Pagel 1989, Rana 1991).Therefore, there is probably a G-dwarf problem also in M32. Lastly, Worthey et al. (1996) found that, in order to match the observed absorption feature Fe4668 in elliptical galaxies, a factor of 4 reduction is required in the number of metal-poor stars predicted by the SM. The same authors also proposed the existence of a universal G-dwarf problem as a viable hypothesis.

However, an ultraviolet excess in the spectral region 2500 to 4000 Å in the integrated spectra of distant ellipticals (with redshifts from 0.3 to 0.45) with respect to the integrated spectra of nearby galaxies was already known in the early eighties (e.g. Oke et al. 1981 and references therein) and was interpreted as a consequence of comparing spectra of whole galaxies with those of nuclear regions. According to this explanation, a G-dwarf problem may exist for central regions but not for the entire galaxy.

In order to provide a contribution to the debated G-dwarf problem in ellipticals, we study in this paper both the global and local G-dwarf problems, related to various metallicity distributions of the stellar component, with the aid of the analytical model (hereafter H model) provided by Hernquist (1990). The qualifier 'global' refers to the galaxy as a whole whereas the qualifier 'local' refers to the projected region within the effective radius R_e.

We follow Ciotti et al. (1995, hereafter CSB) in assuming the existence of a correlation between Z and the stellar binding energy $\mathcal{E}$, but enlarge their approach by considering six $Z-\mathcal{E}$ relations, four of them as single-valued functions $Z(\mathcal{E})$ and two as $\mathcal{E}$-dependent Z spectra. Besides the G-dwarf problem, we also expand the comparison with observations in order to better ensure the consistency of the adopted $Z-\mathcal{E}$ correlations. In particular, we shall consider the profiles of the projected Z values

Send offprint requests to: L. Angeletti

weighted by mass and by luminosity, and the predicted Z distributions of the stars seen along the line of sight and through circular concentric apertures (with respect to the elliptical), together with the integrated colour indices $U-V$, $B-V$, $V-K$, and $1550-V$, and the absorption-line index Mg_2.

The present paper is arranged as follows: in Sect. 2 we recall briefly some basic formulae and properties of the H model and present the $Z-\mathcal{E}$ relations with the corresponding global predictions; the projected mass- and luminosity-weighted mean Z values, the Z distributions of stars seen in projection, and the integrated colour indices are presented in Sect. 3 together with a concise comparison with CSB; the G-dwarf problem and the comparison with the observed correlations $(1550-V)-Mg_2$ and $(U-V)-(V-K)$ are considered in Sect. 4; the discussion and some conclusions are given in Sect. 5. The Appendixes contain the derivation of some formulae used in the text.

2. The H model and the $Z-\mathcal{E}$ relations

In this section we recall only a few technical details of the H model, which are needed throughout the paper, and present our adopted $Z-\mathcal{E}$ relations with the corresponding global predictions. Although the effects of an anisotropic velocity dispersion can be taken into account, we shall adopt the H model in its simplest version, i.e. a spherical and isotropic H model.

2.1. The H model

The H model is defined by the mass-density profile $\rho(r) = aM/[2\pi r(r+a)^3]$ and the potential $\Phi(r) = -GM/(r+a)$, where r is the (spatial) radial distance, a a scale length, G the gravitational constant, and M the total mass of the stellar component (i.e. long-living stars and compact remnants). In the following we shall use the dimensionless positive potential $\psi(r) = -(GM/a)^{-1}\Phi(r)$ and the dimensionless binding energy (per unit stellar mass) $E = (GM/a)^{-1}\mathcal{E}$ with $0 \le E \le \psi_o$ where $\psi_o = \psi(0)$. For the sake of conciseness we shall also adopt M and a as the units of mass and length, respectively.

The projected mass-density profile at the projected radius R reads

$$\rho_p(R) = \frac{1}{2\pi(1-R^2)^2}[(2+R^2)Q(R) - 3] \,, \tag{1}$$

where $Q(R) = (1-R^2)^{-1/2}\ \mathrm{sech}^{-1}R$ for $0 \le R \le 1$, and $Q(R) = (R^2-1)^{-1/2}\sec^{-1}R$ for $1 \le R < +\infty$. The cumulative surface density $\rho_{ap}(R) = 2\pi\int_0^R \rho_p(R')R'\mathrm{d}R'$ within the aperture radius R follows as

$$\rho_{ap}(R) = \frac{R^2}{1-R^2}[Q(R) - 1] \,, \tag{2}$$

and the effective radius R_e, for a constant mass-to-light ratio, turns out to be $R_e \simeq 1.8153$.

We denote by $s(E)$ the cumulative mass of the stars with binding energies not larger than E and normalized to $s(\psi_o) = 1$. Function $s(E)$ is obtained by numerical integration of the equation

$$\frac{\mathrm{d}s}{\mathrm{d}E} = f(E)g(E) \,, \tag{3}$$

where $f(E)$ and $g(E)$ are the distribution function and the density of states, respectively, and are available in terms of elementary functions (see Hernquist 1990). We also denote by $s(Z)$ the cumulative mass of the stars with metallicities not larger than Z, where $Z_{min} \le Z \le Z_{max}$ and $s(Z_{max}) = 1$.

Although the H model closely approximates the $R^{1/4}$-law for ellipticals (Hernquist 1990), such a comparison follows from an adopted constant (i.e. r-independent) mass-to-light ratio, which is not fully consistent with observed colour gradients. Finally, it is assumed that the initial mass function (IMF) is r- and time-independent during the whole phase of star formation.

2.2. The $Z-E$ relations

The observed radial gradients of various colours and spectral indices (considered in Sect. 3) are currently interpreted as due to an underlying gradient of the mean local metallicity of the stellar component, although a contribution from differential dust extinction may be present in elliptical galaxies (Goudfrooij & de Jong 1995). In the spherical and isotropic H model the binding energy is the only free parameter, to which a metallicity spread can be related.

Such a $Z-E$ correlation, which we simply denote by $Z(E)$, is to be thought of as the final outcome of the entire phase of stellar formation. According to current speculations, the galaxy formation may have occurred in a monolithic or fragmentary fashion with various degrees of dissipation, that is in a main episode or through many events, coeval or not. Whatever the correct scenario may be, one can conjecture that the stars, born with the same energy E, also formed with approximately one Z or, alternatively, that they formed with a Z spectrum, eventually depending on E. However, the binding energies of the stars at their birth may not have been equal to their binding energies in the final steady-state of the galaxy.

Therefore, one is faced with two problems. The first one is to recover $Z(E)$ for the steady-state ellipticals we observe today; the second one would be to relate the recovered $Z(E)$ to the epoch before the final virialized state. Since a reliable theory for the galaxy formation is still lacking, we shall only consider the first issue, which is a difficult task in itself, especially so if the existing $Z(E)$ arises from the superposition of several independent $Z(E)$ relations. However, in the following we assume that an elliptical obeys exactly to one $Z(E)$.

In particular, we choose four cases with a single-valued function $Z(E)$ and two further cases with a Z spectrum as a function of E, i.e. Z varies, according to a given law, from a minimum $Z_1(E)$ to a maximum $Z_2(E)$ for any E in $(0, \psi_o)$. Moreover, we shall compare our model predictions with several observational constraints with no pretension, however, of maintaining that all such constraints can ensure the uniqueness of the solution in terms of the $Z(E)$ relation.

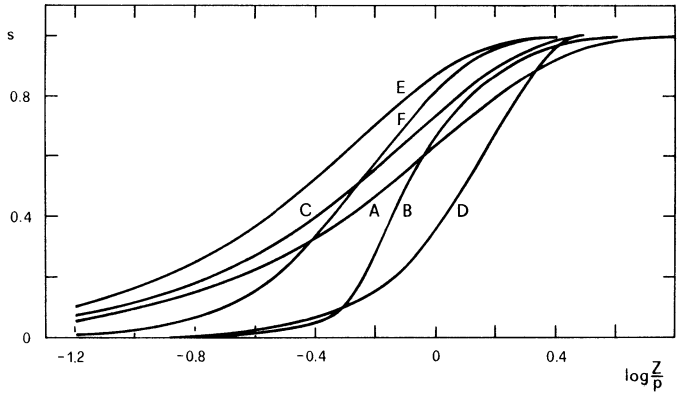

Fig. 1. The global cumu1ative masses $s(Z)$ versus $\log Z/p$ for the labelled models (Sect. 2.2)

All the $Z-E$ relations studied in the following contain the metal yield p as a free parameter. We first consider various models with single-valued functions $Z(E)$.

Model A. The global Z distribution is according to the SM with an initial zero-metal abundance and a star-formation phase lasting until the complete gas exhaustion. We derive $Z(E)$ from $Z(s) = -p\ln(1-s)$ with $s = s(E)$ from Eq. (3).

Model B. The global Z distribution is according to the 'Best Accretion Model' (BAM) of Lynden-Bell (1975; see also Pagel 1989, 1997) with $Z = 0$ for the accreting gas and no gas outflow during the star-formation phase. In the BAM a forming galaxy starts with some gas mass (assumed here with an initial zero-metal abundance) and then grows by gas inflow. The maximum total mass attainable by the stellar component is denoted by M_f (in units of the initial gas mass), which is reached if the gas component vanishes. Assuming the complete gas exhaustion, we derive $Z(E)$ from

$$Z(s) = -p\frac{\ln(1-s)+cs}{(b+cs)^2} ,$$

where $b = 1/M_f$, $c = 1-b$, and $s = s(E)$ from Eq. (3).

We choose the specific value $M_f = 20$, which gives a good fit to the Z distribution of the stars in the solar neighbourhood according to Pagel (1989 and 1997). It should be noted that the BAM reduces to the SM when $M_f = 1$.

Models C and D. The function $Z(E)$ obeys to the power law

$$Z(E) = Z_o E^{1/n} , \tag{4}$$

with $n = 1$ (Model C) or $n = 2$ (Model D), and $Z_o = 3p$, which is approximately the maximum Z attainable in the closed-box computations without the instantaneous recycling approximation.

Models E and F. In the second instance we examine two models, both with $Z_1(E) \le Z \le Z_2(E)$ for any E in $(0, \psi_o)$, and limit ourselves to the choices $Z_1(E) = h_1 p E^{1/n}$ and $Z_2(E) = h_2 p E^{1/n}$, with $h_1 < h_2$. The fractional number of the stars and remnants with a given energy E and abundances not larger than Z is given by

$$N(Z,E) = \int_{Z_1(E)}^{Z^*} \phi(Z',E)\mathrm{d}Z' , \tag{5}$$

where Z^* =min$[Z, Z_2(E)]$ (see the Appendix C). $\phi(Z,E)$ is taken to be

$$\phi(Z,E) = \frac{e^{-(Z-Z_1)/p}}{p[1-e^{-(Z_2-Z_1)/p}]} , \tag{6}$$

with the normalization $\int_{Z_1}^{Z_2}\phi(Z,E)\mathrm{d}Z = 1$, where $Z_1 = Z_1(E)$ and $Z_2 = Z_2(E)$. Model E corresponds to the choice $h_1 = 0$, $h_2 = 3$, and $n = 2$ and Model F to $h_1 = 0.5$, $h_2 = 3$, and $n = 2$. Obviously, F reduces to E for $h_1 = 0$, or to D for $h_1 = 3$.

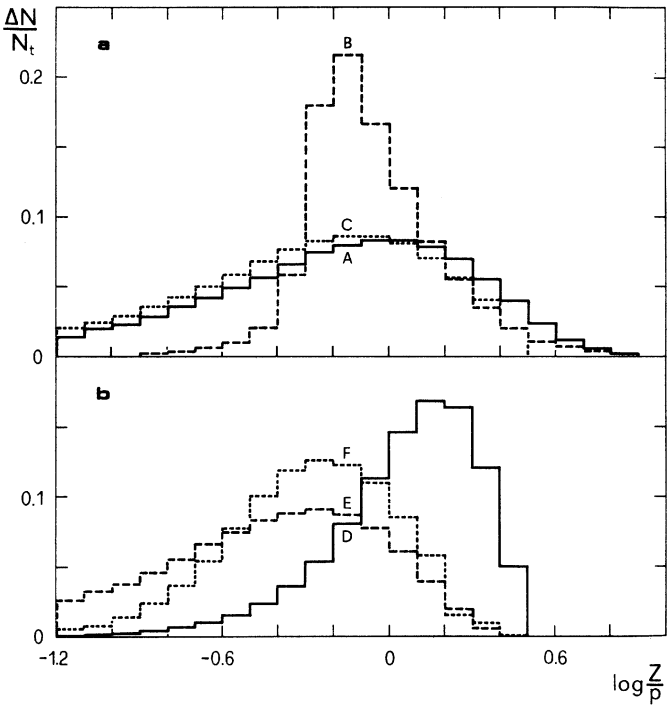

Fig. 2a and b. The global frequency histograms $\Delta N/N_t$ of $\log Z/p$ for the labelled models (Sect. 2.2)

The cumulative masses $s(Z)$ versus $\log Z/p$ are shown in Fig. 1 for the various models, and the corresponding frequency histograms $\Delta N/N_t$ (N_t being the total number of stars and remnants), binned into steps of 0.1 in $\log Z/p$, are shown in Fig. 2a and b. It should be noted that the $Z-E$ relations of Models C to F are adjusted to the specific value $\psi_o = 1$ of the H model; for other spherical models with $\psi_o \neq 1$ (see e.g. Dehnen 1993, Tremaine et al. 1994) they are to be adapted properly.

2.3. Global quantities

The global mass-weighted abundance can be written as $Z_m = \int_0^{\psi_o} z(E)\mathrm{d}s(E)$, where $z(E) = Z(E)$ for Models A to D, and

Table 1. Global values of the mass-weighted Z_m and luminosity-weighted Z_V for the listed models with $s(E)$ from Eq. (3). The Z_V values are given for assumed values of Z_m and refer to the IMF-mass exponent $x = 2.35$; for the other IMF slopes see Sect. 2.3

Mean metallicity	$Z_m/Z_\odot$	A	B	C	D	E	F
Z_m/p	–	1.000	1.000	0.750	1.365	0.505	0.671
$Z_V/Z_\odot$	0.5	0.382	0.455	0.402	0.466	0.400	0.445
”	1.0	0.743	0.901	0.782	0.917	0.780	0.876
”	1.5	1.109	1.360	1.168	1.378	1.169	1.317

Table 2. Global colour indices for the listed models, IMF-mass exponent $x = 2.35$, and assumed values of Z_m (Sect. 2.3)

Index	$Z_m/Z_\odot$	A	B	C	D	E	F	SSP
$U-V$	0.5	1.11	1.21	1.13	1.22	1.13	1.20	1.25
”	1.0	1.21	1.34	1.24	1.35	1.25	1.32	1.41
”	1.5	1.29	1.44	1.31	1.44	1.33	1.41	1.51
$B-V$	0.5	0.84	0.87	0.84	0.87	0.84	0.86	0.88
”	1.0	0.87	0.91	0.88	0.91	0.88	0.90	0.93
”	1.5	0.89	0.94	0.90	0.94	0.90	0.93	0.95
$V-K$	0.5	2.88	2.99	2.91	3.00	2.91	2.97	3.03
”	1.0	3.02	3.15	3.05	3.16	3.05	3.13	3.22
”	1.5	3.10	3.25	3.13	3.25	3.14	3.22	3.31

$z(E) = \int_{Z_1}^{Z_2} Z\phi(Z,E)\mathrm{d}Z$ for Models E and F, with Z_1 and Z_2 depending on E (Sect. 2.2) and $\phi(Z,E)$ as in Eq. (6). The first row in Table 1 lists the Z_m values as obtained with $s(E)$ from Eq. (3). The same table also shows the global luminosity-weighted abundances

$$Z_V = \frac{\int_0^{\psi_o} \zeta_V(E)\mathrm{d}s(E)}{\int_0^{\psi_o} l_V(E)\mathrm{d}s(E)} ,$$

where $s(E)$ is from Eq. (3), and $\zeta_V(E)$ and $l_V(E)$ are defined below. The Z-dependent V luminosities $L_V(Z)$ (per unit mass of the stellar component) are taken from the synthetic single-burst models by Buzzoni (1989, 1995, hereafter B89, B95) for an age of 15 Gyr, a red-horizontal-branch morphology, a mass-loss parameter $\eta = 0.3$, and IMF-mass exponents $x = 1.35$, 2.35, and 3.35 for the stellar masses $\geq 0.1M_\odot$. The quantities $l_V(E)$ and $\zeta_V(E)$ are defined as follows: $l_V(E) = L_V[Z(E)] = L_V(E)$ and $\zeta_V(E) = Z(E)L_V(E)$ in Models A to D, and $l_V(E) = \int_{Z_1}^{Z_2} L_V(Z)\phi(Z,E)\mathrm{d}Z$ and $\zeta_V(E) = \int_{Z_1}^{Z_2} ZL_V(Z)\phi(Z,E)\mathrm{d}Z$ in Models E and F. Table 1 gives Z_V for the values $Z_m/Z_\odot$=0.5, 1, and 1.5, and the Salpeter mass exponent $x = 2.35$. The Z_V values for $x = 1.35$ and 3.35 are within 3% of the values obtained for $x = 2.35$. Table 1 shows that Z_V is 7% to 26% lower than Z_m when $0.5 \leq Z_m/Z_\odot \leq 1.5$ and $1.35 \leq x \leq 3.35$.

Finally, the global colour indices $U-V$, $B-V$, and $V-K$, defined as

$$U - V = (U-V)_\odot - 2.5 \log \frac{\int_0^{\psi_o} l_U(E)\mathrm{d}s(E)}{\int_0^{\psi_o} l_V(E)\mathrm{d}s(E)} ,$$

and the corresponding quantities for $B-V$ and $V-K$, are computed with the Z-dependent luminosities $L_U(Z)$, $L_B(Z)$, $L_V(Z)$, and $L_K(Z)$ (in the U, B, V, and K bands, respectively), which are taken from B89 and B95 (as specified above for the V luminosities; the U luminosities in B89 are corrected according to the recipe given in B95). The quantities $l_U(E)$, $l_B(E)$, and $l_K(E)$ are evaluated as described above for $l_V(E)$; the adopted solar values are $(U-V)_\odot = 0.79$, $(B-V)_\odot = 0.63$, and $(V-K)_\odot = 1.44$, as in B89 and B95.

The colour indices are given in Table 2, with $s(E)$ from Eq. (3) and for $Z_m/Z_\odot$=0.5, 1.0, and 1.5, and $x = 2.35$. They will be compared with observed quantities in Fig. 8 (see Sect. 4.3). The table also lists the colour indices (obtained by interpolation, when necessary, from B89) of Single Stellar Populations (hereafter SSPs) which have the same age (15 Gyr) of Models A to F, and metallicities Z_{SSP} equal to our adopted Z_m values. The table shows that such SSPs are always redder than Models A to F with the maximum differences of about 0.2 mag in $U-V$ and $V-K$, and 0.06 mag in $B-V$. Therefore, the colour indices of A to F can only be matched by SSPs with Z_{SSP} lower than Z_m. For instance, the choice $x = 2.35$ and $Z_m = Z_\odot$ corresponds to $Z_{SSP} \simeq 0.5Z_\odot$ in A, C, and E, $Z_{SSP} \simeq 0.7Z_\odot$ in F, and $Z_{SSP} \simeq 0.8Z_\odot$ in B and D.

3. The projected quantities

In this section we present the radial profiles of the projected metal abundance, along lines of sight at the projected distance R, weighted by the mass and the luminosity L_V, together with the projected profiles of the colour indices $U-V$, $B-V$, and $V-K$. The Z distributions are also estimated for the stars seen through a unit surface at the distances $R = 0.2R_e$, $0.5R_e$, and R_e.

Moreover, we evaluate the Z distributions of the stars seen through circular apertures (concentric with respect to the galaxy) with projected radii $0.2R_e$, $0.5R_e$, and R_e. Finally, the metallicities weighted by mass and by the luminosity L_V, and the colour indices $U-V$, $B-V$, and $V-K$ are computed for the regions within circular concentric apertures with radii $0.2R_e$ and R_e. We shall use $s(E)$ from Eq. (3), the synthetic photometric data from B89 and B95 as specified in Sect. 2.3, and the functions $z(E)$, $\zeta_V(E)$, $l_V(E)$, and the corresponding ones in the other photometric bands, as defined in Sect. 2.3.

3.1. The radial profiles of metallicity and colour indices

We denote by $s_p(E,R)$ the cumulative mass of the stars, seen along the line of sight at the projected radius R, with binding energies not larger than E, and normalized to $s_p[\psi(R),R] = 1$ (see the Appendix A).

Table 3. Mean values of the logarithmic gradients $\Delta \log Z_{m,p}(R)/\Delta \log R$ in the regions within and outside R_e for the listed models (Sect. 3.1)

R/R_e	A	B	C	D	E	F
≤ 1	-0.454	-0.349	-0.417	-0.210	-0.133	-0.169
> 1	-0.850	-0.245	-0.844	-0.422	-0.349	-0.374

Moreover, one has the surface brightness profile in the V band

$$I_V(R) = \rho_p(R) \int_0^{\psi(R)} l_V(E) \mathrm{d}s_p(E,R) \, , \qquad (7)$$

the projected abundances weighted by mass

$$Z_{m,p}(R) = \int_0^{\psi(R)} z(E) \mathrm{d}s_p(E,R) \, ,$$

and by the V luminosity

$$Z_{V,p}(R) = \frac{\rho_p(R)}{I_V(R)} \int_0^{\psi(R)} \zeta_V(E) \mathrm{d}s_p(E,R) \, ,$$

where $\rho_p(R)$ is as in Eq. (1).

The radial profiles of $Z_{m,p}(R)$ are plotted in Fig. 3 for all the models studied. With respect to $Z_{m,p}(R)$ the profiles of $Z_{V,p}(R)$, computed with $p = Z_\odot$, turn out to be shifted downwards by only 1% to 4% in A to D (so that the corresponding curves are practically indistinguishable in Fig. 3) and by amounts indicated by arrows for E and F. The fractional decrease ranges from 20% at the center to 12% at $10R_e$ in E, and is 7% from the center to $10R_e$ in F.

The mean values of the logarithmic radial gradient $\Delta \log Z_{m,p}(R)/\Delta \log R$ are listed in Table 3 for the regions within and outside R_e. The gradient of $\log Z_{V,p}(R)$ coincides practically with that of $\log Z_{m,p}(R)$, except for E, where the mean values are -0.116 and -0.325 for the regions within and outside R_e, respectively.

Fig. 3 shows the relation $Z_{V,p}(R)/Z_\odot \propto (R/R_e)^{-\alpha}$, where $\alpha = \delta/\gamma = 0.32$ follows from the mean slope $\mathrm{d}Mg_2/\mathrm{dlog}(R/R_e) = -\delta = -0.059$ found by Davies et al. (1993) for $R \lesssim R_e$ in a sample of normal and giant ellipticals (see also Carollo et al. 1993), and from an average $\gamma \simeq 0.183$ of $\mathrm{d}Mg_2/\mathrm{d}[Fe/H]$ as provided by the synthetic single-burst models by Worthey (1994) for an age of 15 Gyr, a Salpeter IMF, and a solar relative elemental abundance distribution. The data dispersion of ± 0.022 in δ results in a dispersion of ± 0.12 in α. Finally, Fig. 3 also shows the relation $Z_{V,p}(R)/Z_\odot \propto v_e^{1.47}(R)$, where $v_e(R)$ is the local (i.e. for $r = R$) escape velocity in the H model, which stems from a correlation between Mg_2 and $v_e(R)$, first proposed by Franx and Illingworth (1990). The exponent $1.47 (= \beta/\gamma)$ follows from an average $\beta \simeq 0.27$ of $\mathrm{d}Mg_2/\mathrm{dlog}v_e$, as can be derived from Davies et al. (1993, their Fig. 11a) for the region with $R \lesssim R_e$. Both relations $Z_{V,p}(R)/Z_\odot \propto (R/R_e)^{-\alpha}$ and $\propto v_e^{1.47}(R)$ are extended beyond R_e (without observational support, however) and, for graphical clarity, are shifted vertically by arbitrary amounts. They also suffer from the uncertainties mentioned in the following Sect. 4.2. Fig. 3 shows that, in the region with $R \lesssim R_e$, the curves for A to C have a mean slope $\Delta \log Z_{m,p}(R)/\Delta \log R$ fairly close to that of $(R/R_e)^{-\alpha}$, whereas the curves for D to F have a flatter behaviour, similar to that of $v_e^{1.47}(R)$.

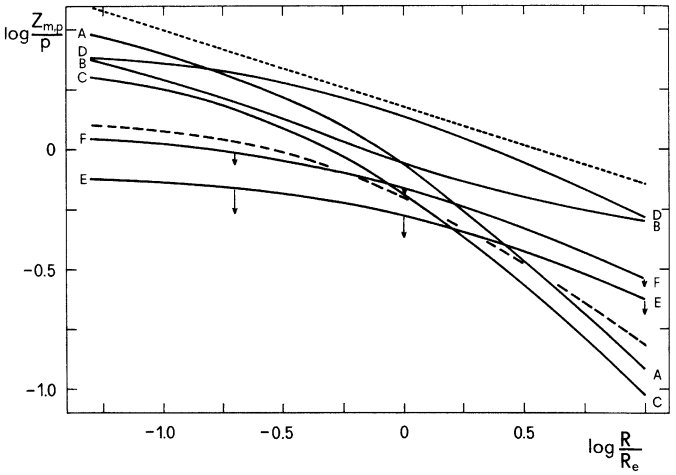

Fig. 3. The radial profiles of the projected mass-weighted abundances $Z_{m,p}(R)$ for $x = 2.35$ and the labelled models. The downward arrows show the displacements of $Z_{V,p}(R)$ with respect to $Z_{m,p}(R)$ in Models E and F. The observational relations $Z_{V,p}(R) \propto (R/R_e)^{-\alpha}$ or $\propto v_e^{1.47}$ are shown in arbitrary units as dotted or dashed curves, respectively (Sect. 3.1)

It appears from Table 3 that there is a fair correlation between the mean metallicity gradients within R_e and the mean slopes of functions $Z(E)$ or $Z_2(E)$ in the range $(0, \psi_o)$, the neighbourhoods of zero and ψ_o being excluded (see also CSB). For example, the mean slope of $Z(E)$ is roughly halved when going from C to D, and the same occurs for the corresponding mean logarithmic gradient of $Z_{m,p}(R)$. Obviously, this point is worthy of a further investigation with a larger set of functions $Z(E)$, $Z_1(E)$, $Z_2(E)$, and $\phi(Z,E)$. Moreover, the above correlations may be useful in modelling the afore-mentioned functions in order to reproduce a given mean metallicity gradient within R_e.

Finally, the projected profiles of the colour indices are evaluated according to

$$(U-V)_p = (U-V)_\odot - 2.5 \log \frac{I_U(R)}{I_V(R)} \, ,$$

and the corresponding quantities for $(B-V)_p$ and $(V-K)_p$, where the surface brightness profiles $I_U(R)$, $I_B(R)$, and $I_K(R)$ in the U, B, and K bands, respectively, are defined by equations analogous to Eq. (7). The colour profiles, computed with $Z_m = Z_\odot$ and $x = 2.35$, are plotted in Fig. 4a–c; the mean values of the radial gradients $\Delta_{U-V} = \Delta(U-V)_p/\Delta \log R$, $\Delta_{B-V} = \Delta(B-V)_p/\Delta \log R$, and $\Delta_{V-K} = \Delta(V-K)_p/\Delta \log R$ are listed in Table 4. In particular, the table shows that $\Delta_{V-K} \simeq \Delta_{U-V}$ and $\Delta_{V-K} \simeq (3 \div 4)\Delta_{B-V}$ inside R_e, whereas $\Delta_{V-K} \simeq (1.45 \div 1.9)\Delta_{U-V}$ and $\Delta_{V-K} \simeq$

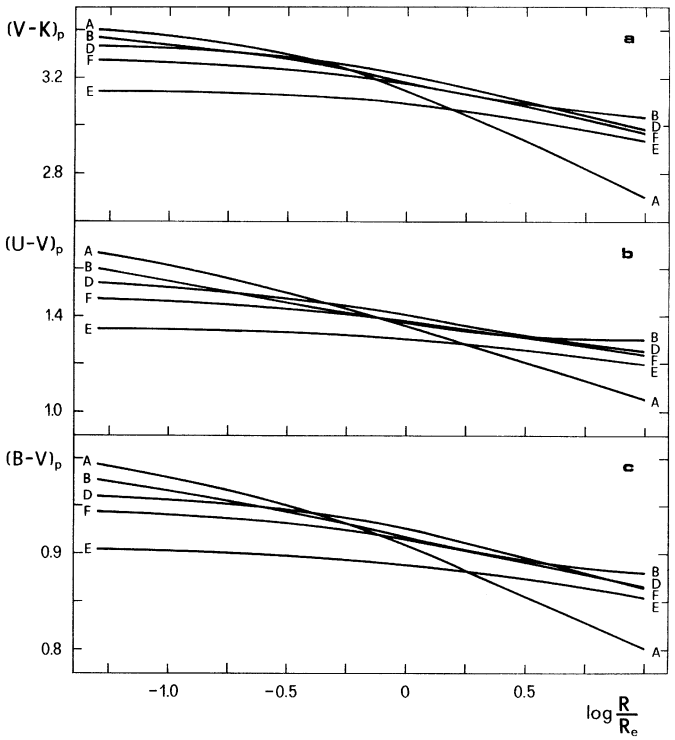

Fig. 4a–c. The radial profiles of the colour indices $(V-K)_p$, $(U-V)_p$, and $(B-V)_p$, with $Z_m = Z_\odot$ and $x = 2.35$, for the labelled models; A overlaps C (Sect. 3.1)

Table 4. Mean values of the colour gradients $\Delta_{U-V} = \Delta(U-V)_p/\Delta\log R$, $\Delta_{B-V} = \Delta(B-V)_p/\Delta\log R$, and $\Delta_{V-K} = \Delta(V-K)_p/\Delta\log R$ in the regions within and outside R_e for the listed models (Sect. 3.1)

R/R_e	Colour gradients	A	B	C	D	E	F
≤ 1	Δ_{U-V}	−0.28	−0.18	−0.27	−0.14	−0.05	−0.10
”	Δ_{B-V}	−0.08	−0.05	−0.08	−0.03	−0.02	−0.03
”	Δ_{V-K}	−0.26	−0.18	−0.26	−0.14	−0.06	−0.11
> 1	Δ_{U-V}	−0.30	−0.08	−0.30	−0.15	−0.10	−0.14
”	Δ_{B-V}	−0.11	−0.04	−0.11	−0.06	−0.04	−0.05
”	Δ_{V-K}	−0.45	−0.15	−0.45	−0.24	−0.15	−0.21

$(3.85 \div 4.45)\Delta_{B-V}$ outside R_e. Such colour gradients agree rather well with those measured (inside R_e) in a sample of 12 ellipticals by Peletier et al. (1990, see their Table 4 and Fig. 10a–c).

3.2. The Z distribution in projection

The binding energies of the stars, seen along the line of sight at the projected radius R, are in the range $0 \leq E \leq E_{max} = \psi(R)$ and the corresponding metal abundances in the range $Z_{min} \leq Z \leq Z_{max}$, where, according to the assumptions in Sect. 2.2, $Z_{min} = 0$ in all the models, and $Z_{max} = Z(E_{max})$ for Models A to D, or $Z_{max} = Z_2(E_{max})$ for Models E and F. Moreover, we denote by $s_p(Z,R)$ the analogue of $s_p(E,R)$ defined in Sect. 3.1, but now with the abundances not larger than Z and normalized to 1 at $Z = Z_{max}$.

In A to D the one-to-one function $Z = Z(E)$ can be inverted to yield $E = E(Z)$ for any given $Z \leq Z_{max}$. One has

$$s_p(Z,R) = \int_0^{E(Z)} \mathrm{d}s_p(E,R) \ .$$

For the remaining two Models E and F one has

$$s_p(Z,R) = \int_0^{E^*} N(Z,E)\mathrm{d}s_p(E,R) \ ,$$

where $N(Z,E)$ is as in Eq. (5), $E^* = \psi(R)$ in Model E and $E^* = \min[E_1(Z), \psi(R)]$ in Model F, $E_1(Z)$ being the inverse function of $Z_1(E)$ (see the Appendix C).

3.3. Projection through circular apertures

We denote by $s_{ap}(E,R)$ the cumulative mass of the stars, seen through a circular concentric (with respect to the galaxy) aperture corresponding to the projected radius R and with binding energies not larger than E, and normalized to $s_{ap}(\psi_o, R) = 1$ (see the Appendix B).

Moreover, one has the cumulative surface brightness in the V band

$$B_V(R) = \rho_{ap}(R) \int_0^{\psi_o} l_V(E)\mathrm{d}s_{ap}(E,R) \ ,$$

and the corresponding expressions for $B_U(R)$, $B_B(R)$, and $B_K(R)$ in the U, B, and K bands, respectively; the projected abundances weighted by mass

$$Z_{m,ap}(R) = \int_0^{\psi_o} z(E)\mathrm{d}s_{ap}(E,R) \ ,$$

and by the V luminosity

$$Z_{V,ap}(R) = \frac{\rho_{ap}(R)}{B_V(R)} \int_0^{\psi_o} \zeta_V(E)\mathrm{d}s_{ap}(E,R) \ ,$$

where $\rho_{ap}(R)$ is as in Eq. (2), as well as the integrated colour index

$$(U-V)_{ap} = (U-V)_\odot - 2.5\log\frac{B_U(R)}{B_V(R)} \ ,$$

and the corresponding quantities for $(B-V)_{ap}$ and $(V-K)_{ap}$.

We also denote by $s_{ap}(Z,R)$ the cumulative mass of the stars, seen through a circular concentric aperture of radius R, and with abundances not larger than Z. The Z values are in the whole range $(0, Z_{max})$ with $Z_{max} = Z(\psi_o)$ or $Z_2(\psi_o)$ (depending on the model considered) and $s_{ap}(Z,R)$ is normalized to 1 at $Z = Z_{max}$. It turns out that

$$s_{ap}(Z,R) = \int_0^{E(Z)} \mathrm{d}s_{ap}(E,R)$$

in Models A to D, and

$$s_{ap}(Z,R) = \int_0^{E^*} N(Z,E)\mathrm{d}s_{ap}(E,R)$$

Table 5. Mass-weighted metal abundances through circular concentric (to the galaxy) apertures with two radii R for the listed models. $Z_{m,ap}(R)/Z_\odot$ is given for assumed global values of Z_m (Sect. 3.3)

Mean metallicity	R/R_e	$Z_m/Z_\odot$	A	B	C	D	E	F
$Z_{m,ap}(R)/p$	0.2	-	2.777	2.219	1.755	2.263	0.729	1.034
”	1.0	-	1.649	1.395	1.190	1.839	0.641	0.876
$Z_{m,ap}(R)/Z_\odot$	0.2	0.5	1.389	1.110	1.170	0.829	0.721	0.770
”	”	1.0	2.777	2.219	2.340	1.657	1.443	1.540
”	”	1.5	4.166	3.329	3.510	2.486	2.164	2.309
”	1.0	0.5	0.825	0.698	0.793	0.674	0.634	0.652
”	”	1.0	1.649	1.395	1.586	1.348	1.269	1.305
”	”	1.5	2.474	2.093	2.379	2.021	1.903	1.957

Table 6. Integrated colour indices through a circular concentric (to the galaxy) aperture with radius R_e for the listed models, with IMF exponent $x = 2.35$ and adopted global values of Z_m (Sect. 3.3)

Index	$Z_m/Z_\odot$	A	B	C	D	E	F
$U-V$	0.5	1.30	1.29	1.31	1.30	1.18	1.27
”	1.0	1.45	1.45	1.47	1.46	1.30	1.41
”	1.5	1.56	1.55	1.58	1.57	1.39	1.52
$B-V$	0.5	0.90	0.89	0.90	0.90	0.86	0.89
”	1.0	0.94	0.94	0.94	0.94	0.90	0.93
”	1.5	0.97	0.97	0.97	0.97	0.92	0.96
$V-K$	0.5	3.10	3.09	3.11	3.10	2.97	3.06
”	1.0	3.26	3.25	3.27	3.28	3.11	3.22
”	1.5	3.34	3.34	3.35	3.36	3.20	3.31

in Models E and F, with $N(Z,E)$ as in Eq. (5), $E^* = \psi_o$ in Model E and E^* =min$[E_1(Z), \psi_o]$ in Model F (see the Appendix C).

The mass-weighted abundances $Z_{m,ap}(R)$ for the central regions seen through circular concentric apertures of radii $0.2R_e$ and R_e are listed in Table 5. For ease of comparison with observational data (see Sects. 4.2 and 4.3), the table also gives $Z_{m,ap}(R)$ when the values $0.5Z_\odot$, $Z_\odot$, and $1.5Z_\odot$ are adopted for the mass-weighted abundance Z_m of the whole galaxy.

The cumulative masses $s_{ap}(Z,R)$, with aperture radii $0.2R_e$, $0.5R_e$, and R_e, are shown in Fig. 5a–c, and the corresponding frequency histograms are displayed in Fig. 6a–f for aperture radii $0.2R_e$ and R_e; they will be discussed in Sect. 4.1.

Finally, the integrated colour indices $(U-V)_{ap}$, $(B-V)_{ap}$, and $(V-K)_{ap}$ of the central region within a circular aperture of radius R_e, computed with $x = 2.35$ and the adopted global values $Z_m/Z_\odot$ =0.5, 1, and 1.5 for the whole galaxy, are listed in Table 6. They will be compared with observed data in Fig. 8 and will be discussed in Sect. 4.3.

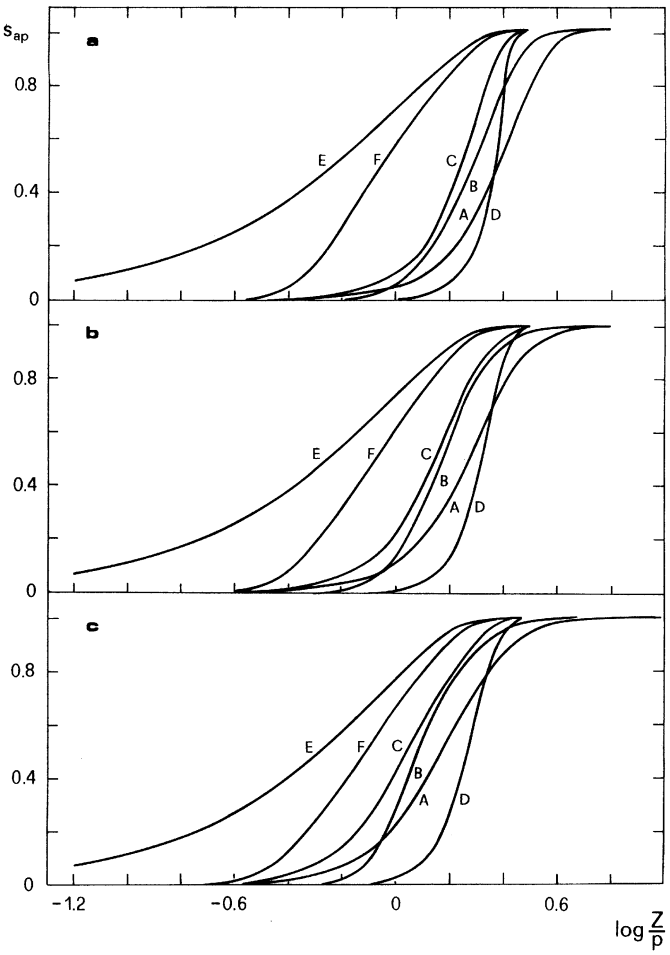

Fig. 5a–c. The cumulative masses $s_{ap}(Z,R)$ of the stars seen through circular concentric (to the galaxy) apertures of radii $0.2R_e$, $0.5R_e$, and R_e (panels **a** to **c**) versus logZ/p for the labelled models (Sect. 3.3)

3.4. Comparison with CSB

We now compare our approach with that adopted by CSB, who applied a well-known inversion procedure to obtain the quantities $\zeta_V(E)$ and $l_V(E)$ from the $R^{1/4}$-law brightness profile $I_V(R)$ and an assumed $Z_{V,p}(R)$ profile, taken by them to be representative of the metallicity gradients measured in ellipticals. When dealing with a one-valued $Z-E$ relation, one has $\zeta_V(E)/l_V(E) = Z(E)$ (see Sect. 2.3). In the case of an E-dependent Z spectrum, however, their procedure does not give explicitely the Z spectrum $\phi(Z,E)$.

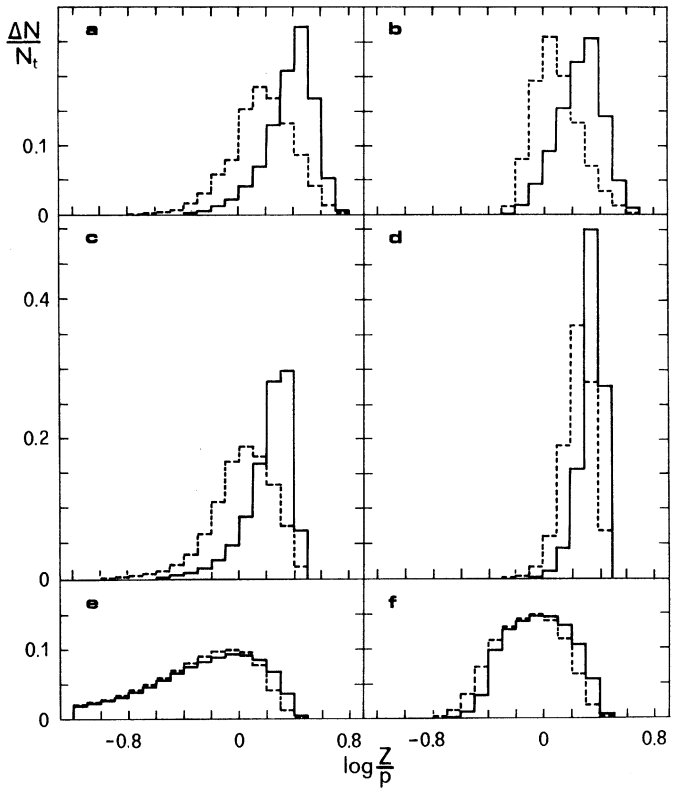

Fig. 6a–f. The frequency histograms $\Delta N/N_t$ of $\log Z/p$ for the stars seen through circular concentric (to the galaxy) apertures of radii $0.2R_e$ and R_e (solid and dashed curves, respectively) for the Models A to F, which label the panels (Sect. 3.3)

In the present paper a reverse approach is adopted, i.e. we start from a set of $Z-E$ relations and then compute, besides the profiles $I_V(R)$ and $Z_{V,p}(R)$ considered by CSB, a certain number of further observable quantities, such as those discussed so far and the profiles of several spectral indices to be presented in a forthcoming paper. A comparison of the computed quantities with those measured in ellipticals can give some indications on the metallicity distributions $Z(E)$ or $\phi(Z,E)$.

Moreover, no attempt is made here to link the adopted $Z-E$ relations to conceivable scenarios of galaxy formation. However, the $Z(E)$ obtained by CSB for the dissipative scenario is very close to our Model D and has a very similar behaviour. Finally, Models C and D have a quasi-linear $Z(E)$ in a wide range of E values, and their slopes correlate fairly well with that of $Z_{V,p}(R)$, as reported by CSB.

4. Further comparisons with observations

In Sect. 3.1 we have found that the radial profile of the abundance $Z_{V,p}(R)$ and the colour indices $(U-V)_p$, $(B-V)_p$, and $(V-K)_p$ compare rather well with those observed in ellipticals. In this section we carry on the comparison with observed data and consider more directly the G-dwarf problem, the ultraviolet (UV) excess, and the integrated colour indices $(U-V)$ and $(V-K)$ of the central region within the projected radius R_e.

4.1. The G-dwarf problem

Because of the lack of a precise definition, in quantitative terms, for the G-dwarf problem in ellipticals, we proceed as follows. Firstly, we consider the ultraviolet spectra referred to in Sect. 1, coming mostly, but not exclusively, from the nuclear regions (see e.g. Dorman et al. 1995 and references therein), as being representative of the projected region inside R_e. Secondly, from the results by TCBF (see e.g. their Figs. 13 and 18) we infer that the flux excess in the spectral region 2000 to 3500 Å can be removed in the galactic models when the percentage of stars with $Z \leq 0.5Z_\odot$ does not exceed 10%. Failing secure information to the contrary, we shall consider the G-dwarf problem with reference to the specific metallicity $0.5Z_\odot$. Therefore, we assume, by analogy with the solar neighbourhood (Pagel 1989 and 1997, Wyse and Gilmore 1995, Rocha-Pinto and Maciel 1996), that a given model presents a global G-dwarf problem if $s(0.5Z_\odot) > 0.1$, and a local G-dwarf problem if $s_p(0.5Z_\odot, R) > 0.1$ or $s_{ap}(0.5Z_\odot, R) > 0.1$ for $R \leq R_e$.

We first consider the global G-dwarf problem. One finds that the condition $s(0.5Z_\odot) < 0.1$ required in order to avoid the global G-dwarf problem is met by A for $p \geq 4.7Z_\odot$, C for $p \geq 6.1Z_\odot$, B and D for $p \geq Z_\odot$, E for $p \geq 8Z_\odot$, and F for $p \geq 2.5Z_\odot$. The same requirement would also imply that Z_m has the following lower bounds: $4.7Z_\odot$, $Z_\odot$, $4.4Z_\odot$, $1.3Z_\odot$, $4.0Z_\odot$, and $1.63Z_\odot$ for A to F, in that order, as can be obtained from Table 1 and Fig. 1. According to current estimates, such Z_m values are exceedingly large in A, C, and E, whereas they seem acceptable in all the remaining models.

Our adopted definition of the global G-dwarf problem implies that $Z_m \geq 0.5Z_\odot$, with the lower limit for an almost monometallic elliptical. Therefore, one can try to further diminish the above lower bounds of Z_m in the favourable Models B, D, and F by changing the free parameters while keeping the condition $s(0.5Z_\odot) \leq 0.1$. It is found that an increase of M_f in Model B is practically ineffective, whereas a lowering of Z_m is possible in generalized versions of Models D and F. Indeed, by adopting $n = 10$ in Eq. (4), the generalized D model has Z_m lowered to $0.59Z_\odot$. Similarly, generalized F models lower Z_m to $1.1Z_\odot$ for $n = 10$ when $h_1 = 0.5$, or from $1.43Z_\odot$ for $n = 2$ to $0.8Z_\odot$ for $n = 10$ when $h_1 = 1$. Clearly, the functions $Z(E)$, $Z_1(E)$, and $Z_2(E)$ become steeper and steeper in the neighbourhood of $E = 0$ for increasing values of n, but also flatter and flatter for larger values of E. The above discussion suggests that, in order to avoid the global G-dwarf problem without resorting to exceedingly large p and Z_m values, a very steep behaviour of $Z(E)$, $Z_1(E)$, and $Z_2(E)$, like that shown by B, would be required in a neighbourhood of $E = 0$.

We now consider the local G-dwarf problem and refer to Fig. 5a–c. For the sake of simplicity, we first assume $Z_m = Z_\odot$ for all the models studied, thus implying that p varies by a factor of 2.7 in the range $(0.76Z_m, 2.04Z_m)$. One finds that all models, except E, can avoid the local G-dwarf problem since they meet both conditions $s_p(0.5Z_\odot, R) < 0.1$ and $s_{ap}(0.5Z_\odot, R) < 0.1$ for $R \leq R_e$. In summary, there is no local G-dwarf problem when $Z_m \geq Z_\odot$, except for E. For $Z_m < Z_\odot$ (but

$\geq 0.5Z_\odot$) there is only a minor difficulty for Model C when $Z_m < 0.75Z_\odot$; a more serious difficulty is encountered by Model F, which can, however, be easily overcome in generalized versions of F, by increasing the parameters h_1 and/or n.

In conclusion, a model of an elliptical galaxy may present: i) neither a global, nor a local G-dwarf problem (e.g. B, D, and F); ii) a global G-dwarf problem but not a local one (e.g. A and C); iii) both a global and a local G-dwarf problem (e.g. E).

By adopting the more favourable values of Z_m found above for removing the local G-dwarf problem, we shall consider all the frequency histograms in Fig. 6a–f, except those referring to E. The histograms, all without low-Z star excesses, show that the Z distributions may differ from each other with respect to the peak values, the narrownesses of the Z distributions around the peak values, and the shapes of the low- or high-Z tail. Such differences are expected to have some consequences on the integrated spectrum. In particular, the shape and extension of the high-Z tail may be relevant to the rising branch of the UV spectrum (below 2000 Å) of elliptical galaxies (see TCBF), as suggested by the observed correlation between the UV − optical colour index $(1550 - V)$ and the spectral index Mg_2.

4.2. The UV excess

In order to compare our model predictions with the observed $(1550 - V) - Mg_2$ relation as given by Burnstein et al. (1988, hereafter B3FL; see also Dorman et al. 1995), we compute both indices $(1550 - V)_{ap}$ and $(Mg)_{ap}$ for the central region seen through a circular concentric aperture of radius $0.2R_e$, which turns out to be a fair approximation to the physical sizes of the central regions observed by B3FL. The SSP indices $(1550 - V)$ and Mg_2, both for $x = 2.35$, are taken from TCBF and Bressan et al. (1996), respectively (note, however, that we use, for $Z = 0.1$ and 15 Gyr, the SSP data for $Z = 0.1$ and 13 Gyr). For each SSP with the abundance Z we derive, by adopting the same calibration as in B3FL, the mean fluxes $F_{UV}(Z)$ and $F_V(Z)$ per unit mass of the stellar component in the 1250-1850 Å region and the V band, respectively. The integrated index $(1550-V)_{ap}$ is

$$(1550 - V)_{ap} = -2.5 \log \frac{\int_0^{\psi_o} f_{UV}(E) \mathrm{d}s_{ap}(E,R)}{\int_0^{\psi_o} f_V(E) \mathrm{d}s_{ap}(E,R)} \ ,$$

where $f_{UV}(E)$ and $f_V(E)$ are related to $F_{UV}(Z)$ and $F_V(Z)$ as, e.g., $l_V(E)$ is related to $L_V(Z)$ (see Sect. 2.3).

For the integrated index $(Mg_2)_{ap}$ we follow the same procedure as that adopted by Greggio (1997). Therefore, for each SSP with the abundance Z, we evaluate the quantities, per unit mass of the stellar component, $F_1(Z) = 10^{-0.4(Mg_2 - BC_V)}$ and $F_2(Z) = 10^{0.4BC_V}$, where BC_V is the bolometric correction to the V-band magnitude, and the related quantities $f_1(E)$ and $f_2(E)$, thus obtaining

$$(Mg_2)_{ap} = -2.5 \log \frac{\int_0^{\psi_o} f_1(E) \mathrm{d}s_{ap}(E,R)}{\int_0^{\psi_o} f_2(E) \mathrm{d}s_{ap}(E,R)} \ .$$

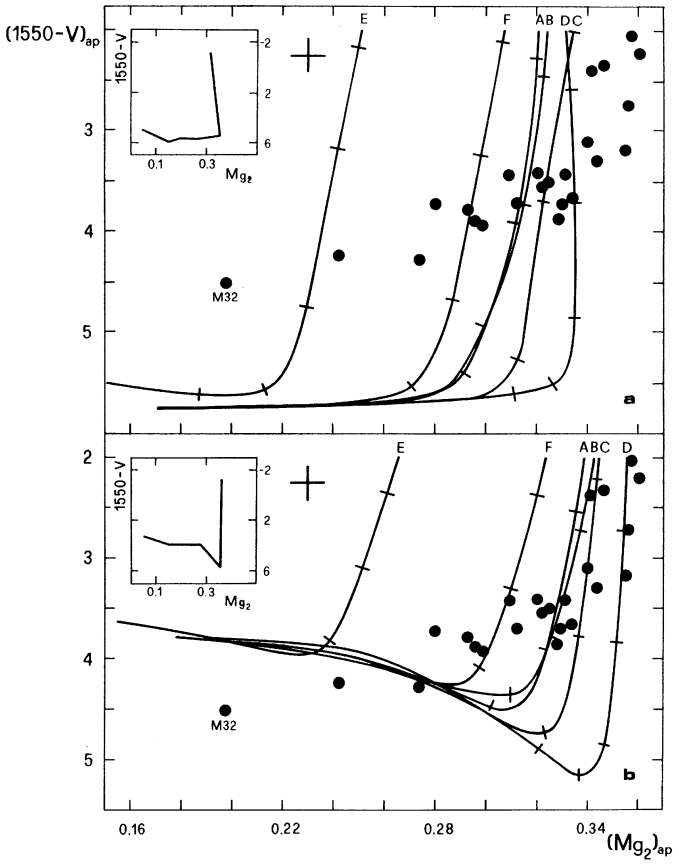

Fig. 7a and b. The integrated colour index $(1550 - V)_{ap}$ versus the integrated absorption-line index $(Mg_2)_{ap}$, through a circular concentric aperture of $0.2R_e$ radius, for the labelled models at the ages of 11.5 Gyr (panel **a**) and 15 Gyr (panel **b**). The tick marks indicate decreasing values (from right to left) of Z_m with steps of $0.25Z_\odot$, starting from $Z_m/Z_\odot$=1.25, 1.5, 1.5, 2.25, 1.75, and 1.5 for Models A to F, in that order. The galaxy data (filled circles) and error bars are from B3FL. The insets show the SSP values of $(1550 - V)$ and Mg_2, from TCBF and Bressan et al. (1996), for the IMF slope x=2.35. The model metallicity $Z_{m,ap}(0.2R_e)$ decreases, along each model sequence, from right to left (Sect. 4.2)

The results are shown in Fig. 7a and b together with the galaxy data from B3FL, for the age of 11.5 Gyr (Feast and Catchpole 1997, Gratton et al. 1997) in panel a, and 15 Gyr in panel b. In each panel, the inset shows the SSP values of Mg_2 and $(1550 - V)$ for the indicated ages. The abundances $Z_{m,ap}(0.2R_e)/Z_\odot$, corresponding to the starting values of Z_m listed in the caption of Fig. 7a and b, can be inferred from Tables 1 and 5; they are 3.1, 3.0, 3.5, 3.7, 2.5, and 2.3 for Models A to F, in that order.

At both ages, $(Mg_2)_{ap}$ does not enter the range $\gtrsim 0.34$ (Model D barely reaches 0.355 at 15 Gyr) which is typical for the strongest UV sources. Our model values of $(Mg_2)_{ap}$ is always lower by at least 0.02 mag (depending on the metallicity dispersion) than the SSP index Mg_2 with $Z_{SSP} = Z_{m,ap}(0.2R_e)$ (see Greggio 1997). Moreover, the SSP values of Mg_2 for $Z_{SSP} = 0.05$ and 0.1 are equal to 0.346 and 0.314 at 11.5 Gyr, and 0.355 and 0.359 at 15 Gyr, respectively. Therefore, in

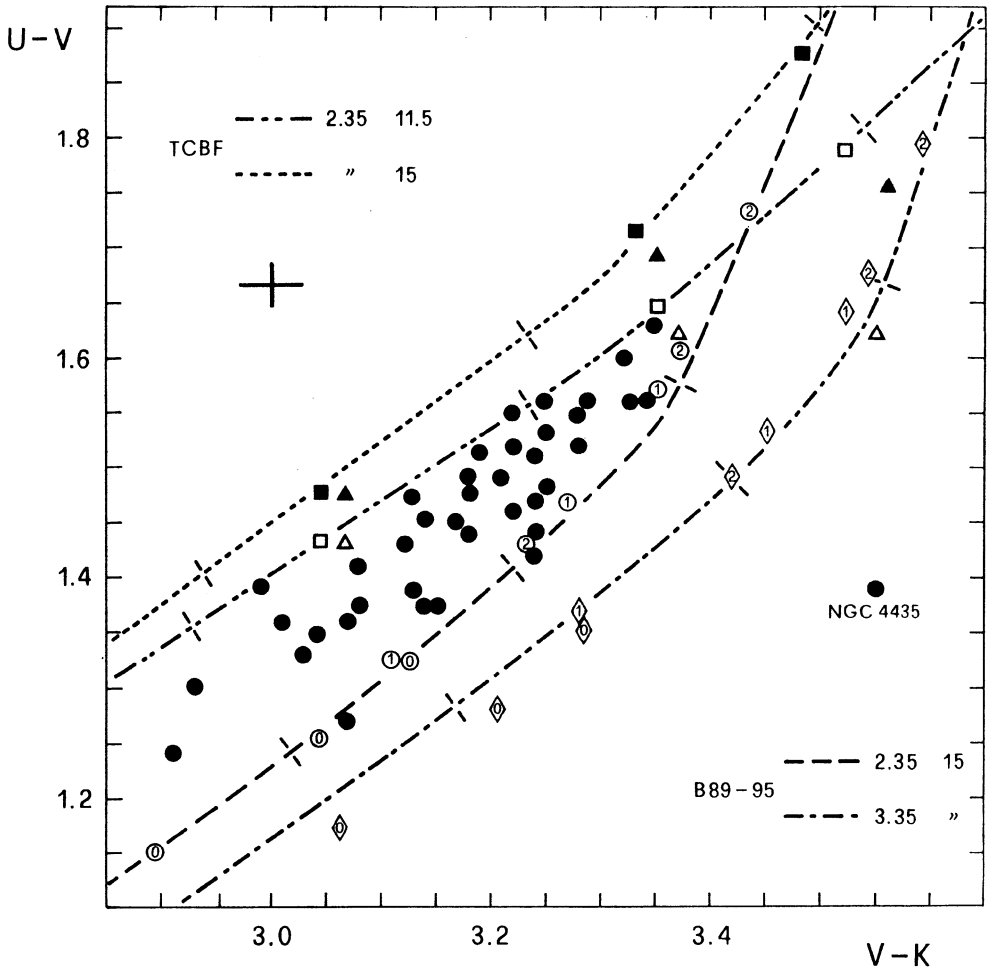

Fig. 8. The galaxy data (filled circles) and error bars are from Bower et al. (1992). Symbols are: *open circles* for a 15 Gyr old Model A with an IMF slope $x = 2.35$, SSP photometric data from B89-95, for the whole galaxy (index 0), the regions projected within R_e (index 1), and $0.2R_e$ (index 2); *open diamonds*, as for the open circles, but with $x = 3.35$; *open (filled) triangles* for a 11.5 Gyr (15 Gyr) old Model A with $x = 2.35$, SSP photometric data from TCBF, and for the region projected within R_e; *open (filled) squares*, as for the open (filled) triangles, but for Model D. In each triad with the same symbols, the bottom-middle-upper locations correspond to $Z_m/Z_\odot$=0.5, 1.0, and 1.5, respectively. The curves give the SSP sequences from B89-95 and TCBF for the x and age values as indicated; the tick marks correspond to log $Z_{SSP}/Z_\odot = -0.3$, 0, and 0.3 from left to right in that order (Sect. 4.3)

order to account for observations (TCBF, Greggio 1997, Weiss et al. 1995), a supersolar Mg/Fe ratio seems to be required at the age of 11.5 Gyr, and also at 15 Gyr for the models other than D, unless only stars with $Z > 0.05$ are present in the galaxy nuclei with the strongest UV emission. Model E appears to be inconsistent with observations, unless a supersolar Mg/Fe ratio is invoked so as to increase Mg_2 by 0.1 mag.

The plateau at $(1550 - V)_{ap} \simeq 5.7$ in Fig. 7a would be shifted upwards to the observed level by adding about 3% of the stars with $Z > 0.05$, i.e. a slightly more extended high-Z tail would be sufficient to fit observations; a roughly similar addition is also required for better fitting galaxy data with $3 \lesssim (1550 - V)_{ap} \lesssim 4$ in Fig. 7b.

Obviously, all above considerations depend on the TCBF approach to the UV upturn in ellipticals (fully detailed in Bressan et al. 1994; see also Greggio and Renzini 1990, Dorman et al. 1995) and on the evolutionary tracks, model atmospheres, and spectral library used by the authors (see Charlot et al. 1996). Moreover, nothing can be said about model results with x other than 2.35, owing to the lack of corresponding SSP data.

As a concluding remark, it should be noted that the observed UV fluxes in ellipticals are spatially extended (Oke et al. 1981, Dorman et al. 1995 and references therein) with a de Vaucouleurs-like profile. Strong UV colour gradients are also observed in some ellipticals (O'Connell et al. 1992). These data could provide a more stringent constraint (not exploited here) to shape the $Z(E)$ relation. In particular, the high Z-tail of $Z(E)$, i.e. for E in a suitable neighbourhood of ψ_o, is expected to have a major impact on the UV colour gradients.

4.3. Colour indices within R_e

Fig. 8 gives the colour indices $U - V$ and $V - K$ (and their estimated mean errors) as measured by Bower et al. (1992) in a sample of 40 Virgo and Coma ellipticals with aperture radii of $30''$ and $5''.5$ respectively, corresponding to the average physical radius R_e (with the standard deviation of $0.64R_e$) for the sampled ellipticals in both clusters. Fig. 8 also shows the colour indices of our Model A, for $x = 2.35$ and 3.35, at 15 Gyr, and referring to the whole galaxy and to aperture radii R_e and $0.2R_e$, with some of the corresponding mean metallicities given in Tables 1 and 5. It turns out that A follows fairly closely the B89-95 SSP sequences (displayed in Fig. 8) with the same input x's and ages, although Z_{SSP} can differ appreciably from our mean metallicities at the same positions in Fig. 8 (see Sect. 2.3).

For a further comparison with galaxy data, the colour indices of Models A and D are computed using SSP data from TCBF

with their adopted $(U-V)_\odot = 0.79$ and $(V-K)_\odot = 1.51$, and for $x = 2.35$, ages of 11.5 and 15 Gyr, and aperture radius R_e. They are displayed in Fig. 8 together with the corresponding SSP sequences by TCBF. It turns out that models containing a proper percentage of stars with $Z > 0.05$ (e.g. Model A at $Z_m = 1.5Z_\odot$) can deviate considerably from the corresponding SSP sequences, owing to the marked decrease of the $U-V$ colour at $Z_{SSP} > 0.05$ with respect to the general behaviour for $Z_{SSP} < 0.05$.

Taking into account the well-known uncertainties in the SSP spectral evolution modelling (Charlot et al. 1996), B89-95 and TCBF appear to reproduce fairly well the observed two-colour slope of galaxy data. However, a conceivable spread of the IMF slopes in ellipticals (Angeletti and Giannone 1997) would be accounted for by the TCBF sequences, but would not by those in B89-95, whose sequence with $x = 3.35$ is well outside the domain of the two-colour data. Moreover, Model A, with an aperture R_e and an age of 11.5 Gyr, would suggest the ranges $0.5 \lesssim Z_m/Z_\odot \lesssim 1$ and $0.8 \lesssim Z_{m,ap}(R_e)/Z_\odot \lesssim 1.6$ for the galaxy data according to TCBF; whereas the same model, with an aperture radius R_e, $x = 2.35$, and an age of 15 Gyr would give the ranges $0.5 \lesssim Z_m/Z_\odot \lesssim 1.5$ and $0.8 \lesssim Z_{m,ap}(R_e)/Z_\odot \lesssim 2.4$ after B89-95.

Our models with $x = 2.35$ not explicitely mentioned above, and all our models with $x = 1.35$, are located very close to the displayed model sequence with $x = 2.35$: for reasons of clarity they are omitted in Fig. 8. Moreover, it should be noted that Buzzoni's data for $Z_{SSP} = 0.1$ and ages other than 15 Gyr are not available, and that the TCBF data for $Z_{SSP} = 0.1$ at 15 Gyr are extrapolated from those in the range 11 to 13 Gyr.

5. Discussion and conclusions

In this paper we address the metallicity distribution and the G-dwarf problem in elliptical galaxies with the aid of the analytical H model. We use a few simple $Z-E$ relations represented by single-valued functions $Z(E)$ or E-dependent Z spectra for each value of the binding energy in the range $(0, \psi_o)$. The aim of our appoach is to gain some preliminary insights on how to formulate a realistic stellar Z distribution that solves the local and/or the global G-dwarf problem and agrees, at the same time, with all major observational findings. Among the observational results we consider the metallicity and colour radial gradients together with the $(U-V)-(V-K)$ and $(1550-V)-Mg_2$ correlations. The basic photometric ingredients are taken from the SSP data, available in the literature, that contain all the necessary information together with an adequate grid of metallicities (up to $Z = 0.1$) and IMF slopes.

Our models, except E, can easily solve the local G-dwarf problem when $Z_m \geq Z_\odot$ with a minor difficulty for Model F when $Z_m < Z_\odot$, which can be easily overcome (Sect. 4.1). The present models can reproduce fairly well the observed metallicity and colour gradients (within R_e). Taking into account the existing uncertainties in the SSP modelling and the likely α-elements enhancement, our models (except E) can also be easily constrained to fit the observed $(U-V)-(V-K)$ and $(1550-V)-Mg_2$ correlations for the regions projected inside R_e and $0.2R_e$, respectively.

As far as the global G-dwarf problem is concerned, we find that Model B can solve it for $Z_m \geq Z_\odot$, Model D for $Z \geq 1.3Z_\odot$, and Model F (with an E-dependent spectrum) for $Z \gtrsim 1.63Z_\odot$. A further lowering of $Z_m (\geq 0.5Z_\odot)$ is possible in generalized versions of Models D and F by increasing the parameters n and/or h_1 (see Sect. 4.1).

We emphasize that, in order to match observational evidences for ellipticals, the G-dwarf problem and the central UV excess have to be considered properly together with the usual metallicity and colour profiles within R_e. In particular, we point out that a specific rising of $Z(E)$, in a neighbourhood of $E = 0$, is expected to solve the global G-dwarf problem (and almost certainly also the local one), in a similar way as the BAM actually does. Moreover, the observed UV fluxes and their gradients can be used to shape precisely the high-Z tail of $Z(E)$ in a convenient neighbourhood of ψ_o. Finally, the familiar metallicity gradients (within R_e) are helpful to model $Z(E)$ in an intermediate range of E values between zero and ψ_o.

We confirm previous findings (Worthey et al. 1996, Greggio 1997) that, owing to the Z dispersion in real ellipticals, the SSP colours and spectral indices cannot be used directly to infer the mean metallicities. We find that the mean metallicities, derived from the SSPs with the same colours and spectral index Mg_2 as found in ellipticals, can be underestimated by up to a factor of 2.

We summarize our main results as follows: i) we use the H model and some probing $Z(E)$ relations, with and without an E-dependent Z spectrum, in order to investigate the chemical structure of ellipticals; ii) we indicate a few simple $Z(E)$ relations that solve the local and/or global G-dwarf problem and agree, at the same time, with the observed radial colours and metallicity profiles, and the $(U-V)-(V-K)$ and $(1550-V)-Mg_2$ correlations; iii) we envisage an operational procedure in order to formulate a $Z-E$ relation that avoids the G-dwarf problem and matches the observed correlations in item ii; iv) we confirm that the mean metallicities, as derived directly from the SSP colours and spectral indices, can be underestimated by up to a factor of 2.

Acknowledgements. We thank M. Friedjung for the english revision of the first version of the paper and an anonymous referee for useful suggestions.

Appendix A: evaluation of $s_p(E, R)$

In order to derive $s_p(E, R)$ we first evaluate the cumulative mass density $\sigma_p(E, R)$ of the stars, seen along the line of sight at the projected radius R, with binding energies not larger than E. It is $\sigma_p(E,R) = 2\int_R^{+\infty} \sigma(E,r)(r^2 - R^2)^{-1/2} r\mathrm{d}r$, where $\sigma(E, r)$ is the mass density of the stars that, at any location r, have binding energies not larger than E. From the relation $\rho(r) = 4\pi \int_0^{\psi(r)} f(E)\sqrt{2[\psi(r) - E]}\mathrm{d}r$, one has: $\sigma(E, r) = \rho(r)$ in the range $r(E) \leq r < +\infty$ and $\sigma(E, r) =$

$4\pi \int_0^E f(E')\sqrt{2[\psi(r)-E']}\mathrm{d}E'$ in the range $R \le r \le r(E)$, where $r(E)$ is the maximum distance to which a star with binding energy E can penetrate. By changing the order of integration, it follows that

$$\sigma_p(E,R) = \int_0^E f(E')J(E',R)\mathrm{d}E' \,, \tag{A1}$$

where

$$J(E,R) = 8\pi \int_R^{r(E)} \sqrt{\frac{2[\psi(r)-E]}{r^2-R^2}} r\mathrm{d}r \,. \tag{A2}$$

The binding energies of the stars seen in projection at R range from zero to $\psi(R)$, so that $\sigma_p[\psi(R),R] = \rho_p(R)$, with $\rho_p(R)$ as in Eq. (1) and $s_p(E,R) = \sigma_p(E,R)/\rho_p(R)$.

Appendix B: evaluation of $s_{ap}(E,R)$

In order to derive $s_{ap}(E,R)$ we first evaluate the cumulative surface mass density $\mu_{ap}(E,R) = 2\pi \int_0^R \sigma_p(E,R')R'\mathrm{d}R'$ of the stars, seen through a circular concentric (with respect to the galaxy) aperture corresponding to the projected radius R and with binding energies not larger than E. From Eqs. (A1) and (A2) one has

$$\mu_{ap}(E,R) = 2\pi \int_0^E f(E') \int_0^R J(E',R')R'\mathrm{d}R'\mathrm{d}E' \,.$$

It results that $2\pi \int_0^R J(E,R')R'\mathrm{d}R'$ is equal to $g(E) - H(E,R)$ for $E \le \psi(R)$, and to $g(E)$ for $E \ge \psi(R)$, where

$$H(E,R) = 16\pi^2 \int_R^{r(E)} \sqrt{2[\psi(r)-E](r^2-R^2)} r\mathrm{d}r \,.$$

One finally obtains

$$\mu_{ap}(E,R) = \int_0^E f(E')g(E')\mathrm{d}E' - \int_0^{E^*} f(E')H(E',R)\mathrm{d}E' \,,$$

with $E^* = \min[E, \psi(R)]$. The binding energies of the stars seen in the aperture considered range from zero to ψ_o, so that $\mu_{ap}(\psi_o, R) = \rho_{ap}(R)$, with $\rho_{ap}(R)$ as in Eq. (2) and $s_{ap}(E,R) = \mu_{ap}(E,R)/\rho_{ap}(R)$.

Appendix C: evaluation of $s(Z)$, $s_p(Z,R)$, and $s_{ap}(Z,R)$

With reference to Models E and F (Sects. 2.2, 3.2, and 3.3), we give a graphical support to the derivation of the cumulative masses $s(Z)$, $s_p(Z,R)$, and $s_{ap}(Z,R)$ from the corresponding cumulative masses $s(E)$, $s_p(E,R)$, and $s_{ap}(E,R)$, respectively.

In all the considered cases, the abundance Z spans the whole range $I_Z = [0, Z_2(E_{max})]$, where $E_{max} = \psi_o$ when treating $s(Z)$ and $s_{ap}(Z,R)$, and $E_{max} = \psi(R)$ when dealing with $s_p(Z,R)$. We denote by E^* the maximum energy E of a star with a given abundance Z in I_Z. In Model E, where $Z_1(E) = 0$, one has $E^* = E_{max}$ (see Fig. 9). In Model F, with $Z_1(E) \neq 0$, one finds: $E^* = E_1(Z)$, $E_1(Z)$ being the inverse function of $Z_1(E)$, when $Z \le Z_1(E_{max})$, and $E^* = E_{max}$ when $Z \ge Z_1(E_{max})$.

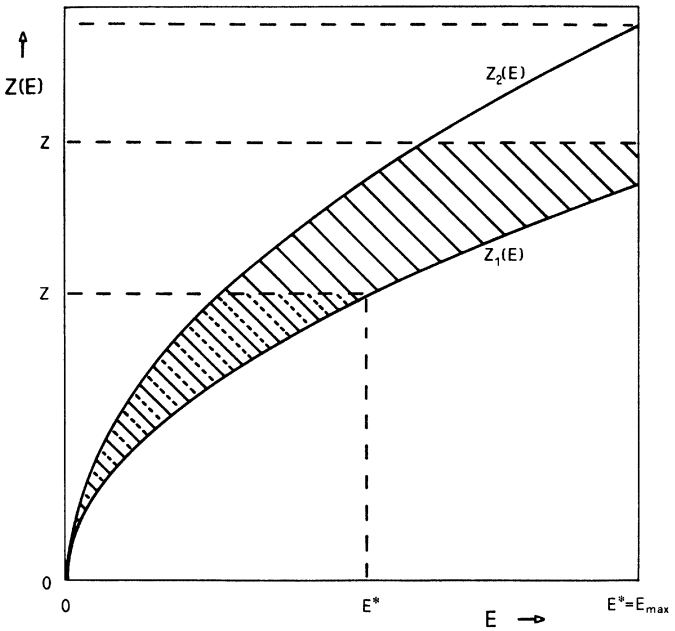

Fig. 9. Domains of integration for Model F, when deriving $s(Z)$, $s_p(Z,R)$, and $s_{ap}(Z,R)$, in the cases $Z \le Z_1(E)$ and $Z > Z_1(E)$ (dotted and dashed areas, respectively). For Model E the dashed area is further enlarged by setting $Z_1(E) = 0$

Let us denote, as in Eq. (5), by $N(Z,E)$ the fractional number of the stars and remnants with a given energy $E(\le E^*)$ and abundances not larger than Z. It turns out from Fig. 9 that

$$N(Z,E) = \int_{Z_1(E)}^{Z^*} \phi(Z',E)\mathrm{d}Z',$$

where $Z^* = \min[Z, Z_2(E)]$, $\phi(Z,E)$ as in Eq. (6), and $Z_1(E) = 0$ in Model E. One finally obtains

$$s(Z) = \int_0^{E^*} N(Z,E)\mathrm{d}s(E),$$

and the corresponding expressions for $s_p(Z,R)$ and $s_{ap}(Z,R)$.

References

Angeletti L., Giannone P., 1997, A&A 321, 343
Bower R.G., Lucey J.R., Ellis R.S., 1992, MNRAS 254, 589
Bressan A., Chiosi C., Fagotto F., 1994, ApJS 94, 63
Bressan A., Chiosi C., Tantalo R., 1996, A&A 311, 425
Burstein D., Bertola F., Buson L.M., Faber S.M., Lauer T.R., 1988, ApJ 328, 440 (B3FL)
Buzzoni A., 1989, ApJS 71, 817 (B89)
Buzzoni A., 1995, ApJS 98, 69 (B95)
Carollo C.M., Danziger I.J., Buson L., 1993, MNRAS 265, 553
Charlot S., Worthey G., Bressan A., 1996, ApJ 457, 625

Ciotti L., Stiavelli M., Braccesi A., 1995, MNRAS 276, 961 (CSB)
Davies R.L., Sadler E.M., Peletier R.F., 1993, MNRAS 262, 650
Dehnen W., 1993, MNRAS 265, 250
Dorman B., O'Connell R.W., Rood R.T., 1995, ApJ 442, 105
Feast M.W., Catchpole R.M., 1997, MNRAS 286, L1
Franx M., Illingworth G.D., 1990, ApJ 359, L41
Goudfrooij P., de Jong T., 1995, A&A 298, 784
Gratton R.G., Fusi-Pecci F., Carretta E., et al., 1997, Proceedings of Hipparcos Venice '97 Symposium, preprint
Greggio L., 1997, MNRAS 285, 151
Greggio L., Renzini A., 1990, ApJ 364, 35
Grillmair C.J., Lauer T.R., Worthey G., et al., 1996, AJ 112, 1975
Hernquist L., 1990, ApJ 356, 359
Lynden-Bell D., 1975, Vistas in Astr. 19, 299
O'Connell R.W, Bohlin R.C., Collins N.R., et al., 1992, ApJ 395, L45
Oke J.B., Bertola F., Capaccioli M., 1981, ApJ 243, 453
Pagel B.E.J., 1989, In: Beckmann J.E., Pagel B.E.J. (eds.) Evolutionary Phenomena in Galaxies. Cambridge University Press, Cambridge, p. 201
Pagel B.E.J., 1997, Nucleosynthesis and Chemical Evolution of Galaxies. Cambridge University Press, Cambridge, p. 201 and 240
Pagel B.E.J., Patchett B.E., 1975, MNRAS 172, 13
Peletier R.F., Valentijn E.A., Jameson R.F., 1990, A&A 233, 62
Rana N.C., 1991, ARA&A 29, 129
Rocha-Pinto H.J, Maciel W.J., 1996, MNRAS 279, 447
Tantalo R., Chiosi C., Bressan A., Fagotto F., 1996, A&A 311, 361 (TCBF)
Tremaine S., Richstone D.O., Byun Y., et al., 1994, AJ 107, 634
Weiss A., Peletier R.F., Matteucci F., 1995, A&A 296, 73
Worthey G., 1994, ApJS 95, 107
Worthey G., Dorman B., Jones L.A., 1996, AJ 112, 948
Wyse R.F.G., Gilmore G., 1995, AJ 110, 2771